Icarus 219 (2012) 77–85

Contents lists available at SciVerse ScienceDirect

Icarus

journal homepage: www.elsevier.com/locate/icarus

Prospects for observing atmospheric gravity waves in Jupiter's thermosphere using H_3^+ emission

Daniel Barrow [a], Katia I. Matcheva [a,*], Pierre Drossart [b]

[a] Department of Physics, University of Florida, P.O. Box 118440, Gainesville, FL 32611-8440, United States
[b] LESIA, Observatoire de Paris, 5 Place Jules Janssen, 92195 Meudon CEDEX, France

ARTICLE INFO

Article history:
Received 18 June 2011
Revised 23 January 2012
Accepted 7 February 2012
Available online 25 February 2012

Keywords:
Atmospheres, Composition
Atmospheres, Dynamics
Ionospheres
Jupiter, Atmosphere

ABSTRACT

We propose the use of H_3^+ thermal emission as a tracer for wave activity present in Jupiter's ionosphere. We model the effect of atmospheric gravity waves on the ion distribution and the H_3^+ thermal emission using a two-dimensional time-dependent model of the wave–ion interaction including ion dynamics, diffusion and chemistry. The model is applied to a broad range of wave parameters to investigate the sensitivity of the observations to the wave amplitude, wavelength, period, and direction of propagation for different latitudes and magnetic field orientations. We find that the impact on the H_3^+ emission is optimized for waves with large vertical and horizontal wavelengths that achieve maximum amplitude at or near the hight of maximum H_3^+ density (roughly 550 km above the 1 bar pressure level). Larger effect is expected from waves with larger amplitudes. Waves that travel in north/south direction are easier to detect than waves propagating zonally. The model also predicts that the largest signal is to come from waves present at middle latitudes.

Our analysis shows that atmospheric gravity waves with parameters consistent with the Galileo Probe observations can leave observable signatures in the H_3^+ thermal emission at 3.4 μm resulting in 5–23% emission variation along the horizontal path of the wave.

1. Introduction

Theoretical models of Jupiter's upper atmosphere (Strobel and Smith, 1973) have demonstrated that solar EUV heating alone fails to account for the high thermospheric temperatures deduced from ground (Drossart et al., 1989, 1993; Ballester et al., 1994; Miller et al., 1997; Stallard et al., 2002; Raynaud et al., 2004a) and space observations (Fjeldbo et al., 1975; Atreya et al., 1979; Seiff et al., 1997).

Several heating mechanisms have been considered as an explanation for this discrepancy in Jupiter's energy budget including soft electron precipitation (Hunten and Dessler, 1977), energetic electrons (Waite et al., 1983; Shemansky, 1985), Joule heating (Nishida and Watanabe, 1981), heavy ion precipitation (Strobel, 1979; Waite et al., 1997), dissipation of upward propagating gravity waves (French and Gierasch, 1974; Yelle et al., 1996; Young et al., 1997; Matcheva and Strobel, 1999; Hickey et al., 2000) and energy transport by dissipating acoustic waves (Schubert et al., 2003). Pinpointing the exact mechanism responsible for the elevated thermospheric temperatures proved to be rather elusive as the parameters of the proposed energy sources are not constrained by observations.

Young et al. (1997) noted the presence of wave-like variations in the temperature profile obtained by the Galileo Probe and interpreted them as signatures of gravity waves. Their calculations showed that the observed wave modes could heat the upper atmosphere sufficiently enough to maintain the high thermospheric temperatures. Subsequent analysis by Matcheva and Strobel (1999) and Hickey et al. (2000) demonstrate that viscous dissipation of gravity waves with parameters consistent with the Galileo Probe temperature profile are insufficient to heat Jupiter's thermosphere to the observed temperatures. It has been pointed out, however, that atmospheric gravity waves with different parameters can potentially have a strong impact on the energy and momentum budget of Jupiter's atmosphere at high altitudes (Matcheva and Strobel, 1999).

Observations of gravity waves on Jupiter to date are limited and are subject to model dependent interpretations. This is especially true for the upper atmosphere where observable tracers are not readily available. The only evidence for wave activity at thermospheric heights comes from the Galileo Probe temperature profile (Young et al., 1997) and from modeling small-scale fluctuations in the electron density in Jupiter's lower ionosphere (Matcheva et al., 2001; Barrow and Matcheva, 2011). In the stratosphere signatures of gravity waves have been deduced from stellar

* Corresponding author.
E-mail addresses: dbarrow@phys.ufl.edu (D. Barrow), katia@phys.ufl.edu (K.I. Matcheva), pierre.drossart@obspm.fr (P. Drossart).

0019-1035/$ - see front matter © 2012 Elsevier Inc. All rights reserved.
doi:10.1016/j.icarus.2012.02.007

occultations (French and Gierasch, 1974; Raynaud et al., 2003, 2004b) and from the Galileo Probe temperature profile (Young et al., 2005). In the troposphere images of Jupiter's equatorial clouds (Hunt and Muller, 1979; Reuter et al., 2007; Arregi et al., 2009) show presence of waves embedded in the zonal mean flow.

The quasi-periodic oscillation of the zonal-mean stratospheric temperature and winds of Jupiter at low latitudes which has been reported in the literature (Leovy et al., 1991; Simon-Miller et al., 2006, 2007) has been successfully modeled as a manifestation of the interaction of atmospheric gravity waves with the mean zonal wind and the background atmospheric state (Friedson, 1999). The potential importance of the wave–mean flow interaction for the momentum transport in the stratosphere has been also pointed in the case of Saturn (Sayanagi and Showman, 2007), where small-scale wave-like activity is detected in stellar occultations (Harrington et al., 2010). Strong vertical shear in the stratosphere can prevent some of the gravity wave modes from reaching high altitudes providing a natural filtering mechanism for the waves at thermospheric heights. Constraining the spectrum of gravity waves present in the jovian thermosphere can shed additional light on the origin of the waves and the nature of the observed stratospheric oscillations.

The observed gravity waves are sparse but cover a wide range of wave parameters with horizontal wavelengths spanning from about 70 km to roughly 13,000 km. The gravity wave contribution to the thermospheric energy budget depends on the parameters of the present gravity waves (amplitude, wavelength, and frequency). It is difficult to estimate the extent to which gravity waves influence the energy budget of Jupiter's upper atmosphere without a better understanding of the extant waves. To correctly estimate the wave contribution to the energy and momentum budget of Jupiter's upper atmosphere an efficient method must be developed to detect the waves and measure their parameters, including the wave amplitude, wavelength, period, direction of propagation, and source region.

Above the homopause Jupiter's atmosphere is dominated by molecular hydrogen and helium and at high altitudes by atomic hydrogen. None of these species allow us to sample the thermal structure of the atmosphere through infrared remote sensing. The dominant ionospheric species in this region are H^+ and H_3^+. Ever since its detection on Jupiter (Drossart et al., 1989) measurements of the emission of H_3^+ ions in the near infrared have been successfully used to estimate the temperature at the H_3^+ peak altitude (Drossart et al., 1993; Ballester et al., 1994; Miller et al., 1997; Stallard et al., 2002; Raynaud et al., 2004a).

In this paper we explore the option to use the H_3^+ near-infrared emission to detect the presence of atmospheric gravity waves in Jupiter's upper atmosphere. We focus on three separate effects that lead to wave signatures in the observable H_3^+ emission: H_3^+ ion temperature variation, H_3^+ ion density variation and H_3^+ ion column density changes as the wave propagates through the atmosphere.

Gravity waves propagating in the ionosphere in the presence of a magnetic field can significantly alter the ionospheric structure near the altitude where the amplitude of the gravity wave peaks. In Jupiter's ionosphere the wave–ion interaction gives rise to the formation of multiple, well-defined layers of ions and to horizontal variations in the ion column densities, particularly that of H_3^+ (Barrow and Matcheva, 2011). In turn, changes in the H_3^+ column density results in variations in the observed H_3^+ thermal emission along the path of the propagating wave. We study the magnitude of this effect using a two-dimensional, time-dependent model of the interaction of atmospheric gravity waves with ions (Barrow and Matcheva, 2011) coupled with a radiative transfer model of Jupiter's near infrared emission at 3.4 μm. Simulations are performed for a broad range of wave parameters (amplitude, horizontal and vertical wavelengths, direction of propagation) and magnetic field orientation.

2. Gravity wave-ionosphere interaction

Atmospheric gravity waves are buoyancy driven, transverse oscillations that propagate in a stably stratified atmosphere. A gravity wave propagating vertically in a conservative atmosphere with a constant zonal wind has a temperature amplitude that increases exponentially with altitude, conserving energy as the background density decreases exponentially. If the wave amplitude grows so large that the temperature gradient exceeds the adiabatic lapse rate the wave breaks, depositing excess energy into the background atmosphere. In reality, waves undergo dissipative processes that limit the amplitude growth. These processes include eddy diffusion, molecular viscosity, thermal conduction, ion drag, and radiative damping. In addition waves can encounter critical regions along their path resulting in reflection or absorption of the waves within the background wind flow. Among the dissipative processes molecular viscosity and thermal conduction become particularly efficient at damping the wave growth at high altitudes. The altitude at which wave dissipation balances the growth of the wave amplitude is referred to as the wave's peak altitude.

A gravity wave can have a pronounced effect on the structure of the ionosphere in the presence of a magnetic field. Fig. 1 illustrates the basic mechanism of the interaction between the neutral atmosphere and the ionized gas as a gravity wave propagates through the region. The wave sets the neutral atmosphere in motion with the gas moving along the wave phase lines. The neutrals in turn drag the ions along. Where the ion-gyro frequency is greater than the ion collision frequency the ions are constrained to move along the magnetic field lines. The resulting ion motion is a projection of the neutral wind $\vec{U}_n$ in the direction of the local magnetic field $\vec{B}$.

$$\vec{U}_i = -\sigma_i \left[\left(\frac{\nabla N_i}{N_i} + \frac{\nabla T_p}{T_p} + \frac{\hat{l}_z}{H_p} \right) \cdot \hat{l}_b \right] \hat{l}_b + (\vec{U}_n \cdot \hat{l}_b)\hat{l}_b. \quad (1)$$

In Eq. (1) the total ion velocity $\vec{U}_i$ is a superposition of the ion diffusion velocity (first term) and the wave induced motion (second term). Here N_i is the ion density, T_p is the plasma temperature, and H_p is the plasma scale height, $\hat{l}_b$ and $\hat{l}_z$ are unit vectors in the direction of the magnetic field and the positive vertical direction, respectively. The symbol σ_i stays for ion diffusion coefficient. With the neutral winds forced by the gravity waves, the ion velocities are set into converging and diverging layers. The described model for creating sharp layers of ions/electrons is known as "wind shear

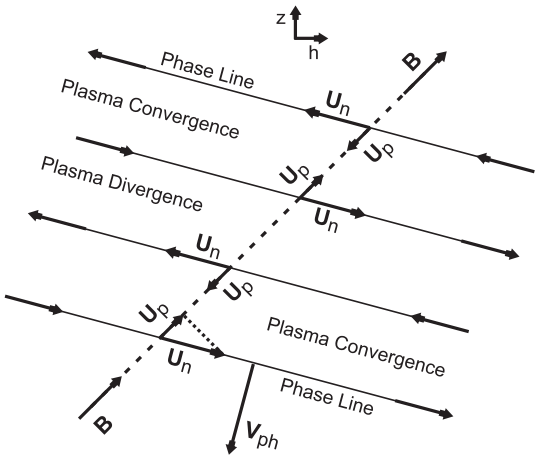

Fig. 1. Ion layering mechanism. The vertically alternating neutral wind field creates layers of plasma flux convergence and divergence. V_{ph} denotes the wave phase-velocity vector. The wave in the diagram is propagating along the magnetic meridian. The plasma velocity vector, U_p, is the projection of the neutral velocity vector, U_n, in the direction of the magnetic field vector B.

mechanism" and it is first proposed as an explanation of the observed traveling ionospheric disturbances typical for the Earth's lower ionosphere at evening hours (Hooke, 1968).

The response of the ion distribution to the presence of waves depends on the ion chemistry. Ions with long lifetimes (greater than the wave period) accumulate to create sharp layers of plasma compression and rarefaction (Hooke, 1970; Davis, 1973; Kirchengast, 1996). On the other hand, short-lived ions are not significantly perturbed by the neutral winds since they do not exist long enough to be notably displaced by the wave. However, an ionized species that undergoes fast chemical reactions with a perturbed, long-lived ion will express similar layering in its density as it tends toward chemical equilibrium with the perturbed, long-lived ion (Barrow and Matcheva, 2011).

Throughout most of the jovian ionosphere the H^+ and the H_3^+ ions fit well the two-ion case scenario for wave–ion interaction. The dominant H^+ ions, that have a long lifetime, are forced into layers by the neutral wind shear, which in turn produces perturbations in the density of the relatively short-lived H_3^+ ions through chemical interactions. The value of this idealized approach is that it allows for an exact solution for the resulting ion density perturbations and illustrates the nature of the wave–ion interaction. Eqs. (2) and (3) (Barrow and Matcheva, 2011) are the analytical solution of the ion continuity equations for small amplitude perturbations in the H^+ and H_3^+ ion density as a result of a passing gravity wave with a wavenumber $\vec{k}$ and frequency ω_0.

$$N_1'(x,y,z,t) = \frac{N_{1o}(\vec{U}_n' \cdot \hat{l}_b)}{\omega_o}\left[\vec{k}_r \cdot \hat{l}_b - i\left(\frac{1}{N_{1o}}\frac{\partial N_{1o}}{\partial z} + \frac{1}{2H^*} - k_{zi}\right)\left(\hat{l}_b \cdot \hat{l}_z\right)\right], \tag{2}$$

$$N_2'(x,y,z,t) = \frac{N_{2o}(\vec{U}_n' \cdot \hat{l}_b)[\omega_o - iL]}{\omega_o^2 + L^2}\left[\vec{k}_r \cdot \hat{l}_b - i\left(\frac{1}{N_{2o}}\frac{\partial N_{2o}}{\partial z} + \frac{1}{2H^*} - k_{zi}\right)(\hat{l}_b \cdot \hat{l}_z)\right] + \frac{[G-L][i\omega_o + L]}{\omega_o^2 + L^2}N_1'. \tag{3}$$

In the equations above N_1 corresponds to the primary (dominant) H^+ ions and N_2 to the secondary (minor) H_3^+ ions. The prime and subscript-o notations denote perturbed and background quantities, respectively. The chemical production and loss rates of the minor ion due to interactions with the dominant ion (and the corresponding electron density) are represented by the G and L terms, respectively. The vector $\vec{k}_r$ is the real part of the wave number and k_{zi} is the imaginary part of the vertical component of the wavenumber of the forcing wave which arises from the dissipation. The symbol H^* is the density scale hight of the neutral atmosphere. The right-hand-side of Eq. (2) is essentially the wave-induced ion flux (including diffusion) divided by the frequency of the forcing wave. For the long-lived H_3^+ ion Eq. (3) includes also the relevant ion chemistry represented by the second term on the right-hand-side.

For long-lived ions the wave–ion interaction moves charges back and forth along the magnetic field lines, creating layers in the ion density but essentially conserving the total ions present. Short-lived, chemically perturbed ions effectively establish chemical equilibrium with other perturbed species instantaneously. The number of short-lived ions is not conserved and so their vertically integrated densities can vary significantly along the horizontal wavelength. This effect in the H_3^+ density will yield variations in the H_3^+ thermal emission that will be observable under certain conditions. In this work we investigate the effect of waves on the H_3^+ thermal emission and evaluate under what planetary conditions and wave parameters the effect will be most pronounced. We couple a gravity wave-ionospheric model (Barrow and Matcheva, 2011) with a radiative transfer model (Drossart et al., 1993) to quantify these effects. The model for this work is described in detail in the following section.

3. Model

To represent the effects of a propagating gravity wave on the ionosphere of Jupiter we employ the model from Barrow and Matcheva (2011). This is a self consistent, atmospheric model based on several modules: (1) neutral atmosphere module, (2) atmospheric gravity wave module, (3) ionosphere module. In this paper we add a radiative transfer module to estimate the observable effect of the waves in the H_3^+ emission. The vertical range of the model spans from 100 km above the 1 bar level to 1500 km with a vertical resolution of 1 km. To resolve the propagating waves we calculate the structure of the atmosphere/ionosphere at 28 points along a single horizontal wavelength. The time step used for the ion–wave interaction module is 50 s.

The following sections overview the model's components and describe the relevant parts in detail. For a complete description of the gravity wave-ionosphere model see Barrow and Matcheva (2011).

3.1. Neutral atmosphere

The model treats the neutral atmosphere as a superposition of a steady state solution (background neutral atmosphere) and a small amplitude time-dependent perturbation (atmospheric gravity wave). The steady state is calculated using an analytical fit to the Galileo Probe temperature profile (Seiff et al., 1997). The mixing ratios of the main neutral constituents (H_2, He, CH_4) are calculated for diffusive equilibrium using the Galileo measurements as a bottom boundary condition (von Zahn et al., 1998; Niemann et al., 1996) and an eddy diffusion coefficient $K = 5 \times 10^6$ cm^2/s (Yelle et al., 1996). The resulting neutral density profiles are in good agreement with the composition model from Seiff et al. (1998). The background neutral atmosphere is kept constant throughout the simulations.

Jupiter's magnetic field has a large influence on the ion dynamics at high altitudes. We incorporate the VIP4 model of Jupiter's magnetic field (Connerney et al., 1998) to represent magnetic field magnitude and orientation for a given location.

3.2. Atmospheric gravity wave model

The atmospheric gravity wave model is based on the WKB solution of the linearized fluid equations for conservation of mass, momentum, and energy using the quasi-Boussinesq approximation in a dissipative atmosphere with slowly varying background temperature and zonal wind. The model is described in detail in Matcheva and Strobel (1999). Dissipation is due to molecular and eddy viscosity and thermal conduction, with eddy dissipation dominating the region below the homopause and molecular processes becoming increasingly more important with altitude.

In absence of dissipation and background wind shear the velocity amplitude of the waves increases exponentially with altitude as the atmospheric density decreases. If the amplitude exceeds a critical value the wave becomes unstable and breaks. We consider only linear waves with amplitudes less than their critical (breaking) value. At high altitudes the growth of the wave amplitude is limited by dissipation. The bottom left panel of Fig. 4 shows the vertical profile of the temperature amplitude of a gravity wave with vertical wavelength of 93 km and a horizontal wavelength of 12,693 km. Below 455 km the wave amplitude is still increasing where as above 455 km the wave amplitude is dominated by dissipation and decreases. We will use the term "wave peak altitude" as

Table 1
Model emission contrast for observed waves.

Observation	λ_h (km)	λ_z (km)	z_{peak} (km)	Period (h)	Contrast (%)
G. Probe 1	12,700	92	455	17.32	23.0
G. Probe 2	800	150	764	1.17	5.02
J0-ingress	500	60	510	1.36	0.86
G. Probe 1*	12,700	131	505	15.46	28.7
G. Probe 2*	2500	150	661	3.41	16.8
J0-ingress*	3500	93	504	5.96	11.1

a reference to the altitude at which the wave amplitude is maximum. Note that wave dissipation does not occur just at a particular pressure level but rather over an extended vertical range. Above the wave peak altitude the wave is strongly dissipated and its signatures are obscured within a scale hight or so.

The gravity wave model that we use produces spatially and temporally varying wind and temperature fields for a given wave amplitude, and vertical and horizontal wavelengths of a gravity wave. The structure of the propagating wave is recalculated every 50 s. The output from the wave model is used to force the ion motion according to Eq. (1).

3.3. Ionospheric chemistry

Our chemical model accounts for six ion species, H^+, He^+, H_2^+, CH_4^+, HeH^+, H_3^+, as well as electrons and maintains 32 charge exchange and recombination reactions, listed with references in Barrow and Matcheva (2011) (please, note that there is an unfortunate typo in the reaction coefficient rates for reactions 24–32 in Table 1 of the reference – in the temperature dependent term the power refers to the entire fraction). Photochemical production and secondary electron ionization of the H^+, He^+, H_2^+, and CH_4^+ ions are also included. Following Cravens (1987) we invoke a charge exchange reaction with vibrationally excited molecular hydrogen to reproduce the observed values for the main electron peak. The ion chemical lifetime and the steady state solution for the vertical ion distribution are presented in Figs. 2 and 3, respectively. The resulting steady state electron density profile compares well with the observations during the Galileo J0 radio occultation (Hinson et al., 1997) with an electron density maximum of 10^5 cm^{-3} and a peak location at 900 km above the 1 bar level. The H_3^+ abundance is maximum at about 550 km above the 1 bar level.

In the lower ionosphere (below 550 km) where the chemistry of the H^+ and the H_3^+ ions is dominated by charge exchange reactions with CH_4 molecules the two major ions are relatively short lived and have comparable abundances. Above 600 km the H_3^+ lifetime is limited by its fast recombination with ambient electrons. In contrast, the H^+ ions recombine slowly which renders the H^+ ions as the dominant ion at these altitudes. Clearly above 600 km Eqs. (2) and (3) are well suited to describe the interaction of the long-lived H^+ ions with atmospheric gravity waves and the subsequent impact on the density of the short-lived H_3^+ ions. This is not the case for the bottom of the ionosphere ($z < 500$ km). The chemical lifetime of all ions is short in comparison with typical gravity wave periods, which for Jupiter's thermosphere range between 15 min and a few hours.

The steady state solution is used to initialize our time-dependent system of continuity equations (Barrow and Matcheva, 2011) which solve for the evolution of the ion densities in two dimensions (one vertical and one horizontal). In contrast to the analytical approach outlined in Section 2 the numerical model has no limitations for the ion lifetime and/or the magnitude of the ionospheric response. The two approaches agree at the small amplitude limit (Barrow and Matcheva, 2011). The only restriction of the numerical model is that the ion gyro frequency should exceed the ion collision frequency, a condition satisfied above the altitude of 450 km above the 1 bar pressure level.

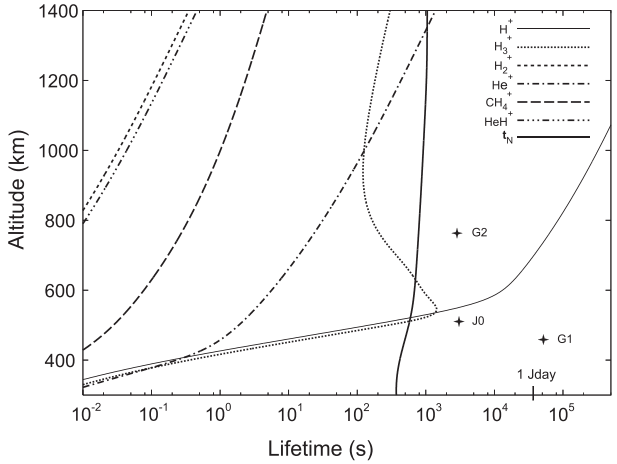

Fig. 2. Ion lifetimes. The chemical lifetimes of the ions included in the model are shown using the following line stiles: H^+ thin solid line; H_3^+ thin dotted line; H_2^+ thick dotted line; He^+ dash-dot line; CH_4^+ dashed line; HeH^+ dash-triple dot line. The buoyancy period (thick solid line) and the duration of one jovian day are displayed for reference. The periods of three observed waves (J0, G1, and G2) are labeled at the altitudes at which they peak. For the wave parameters see Table 1.

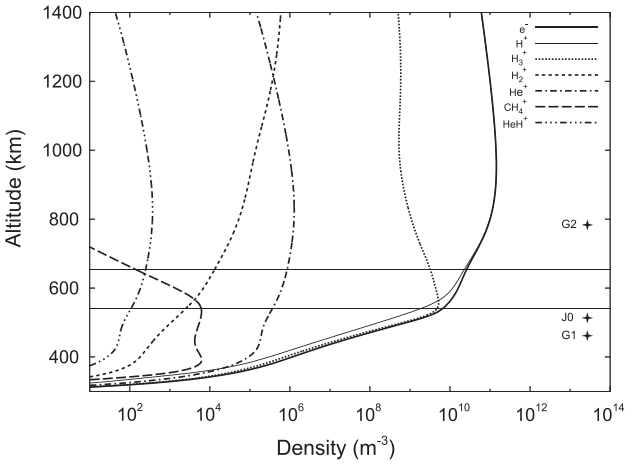

Fig. 3. Background ion densities. Model steady state ion densities in the absence of atmospheric gravity waves (e^- thick solid line; H^+ thin solid line; H_3^+ thin dotted line; H_2^+ thick dotted line; He^+ dash-dot line; CH_4^+ dashed line; HeH^+ dash-triple dot line). Here the model assumes diurnally averaged photochemical production. The horizontal solid black lines encompass the vertical range of the background H_3^+ density peak. The peak altitudes of three observed waves (J0, G1, and G2 - see Table 1) are also shown.

3.4. H_3^+ emission

Emission from H_3^+ was first detected from Jupiter in 1988 (Drossart et al., 1989). The spectroscopy of H_3^+ vibro-rotational band in L band is fully described in Kao et al. (1991). The ν_2 band of H_3^+ is observed (Weak hot band lines have been detected, but play a marginal role in the emission). The H_3^+ emission model used in the paper is a line-by-line calculation in a LTE optically thin regime. This approximation has been extensively and successfully used in past interpretations of H_3^+ observations (e.g. Drossart et al., 1989) including some at a high spectral resolution resolving the line width of the emission (Drossart et al., 1993). Non-LTE effects have been discussed by Melin et al. (2005), and can affect the retrieved abundance of H_3^+, but would not affect the order of

magnitude of the presented results, where variability of the emission is the observable parameter, and not the absolute magnitude of the emission. In the optically thin regime, scattering of H_3^+ photons by self-absorption or particulates is negligible, as no scatterers are present at this altitude on Jupiter. At the pressure regime of the ionosphere the Doppler broadening of the emission lines is dominant whereas the pressure broadening is negligible.

The H_3^+ ion has been recognized as having substantial utility as a tracer to learn about the thermal and the dynamic state of the ionosphere of giant planets (Miller et al., 1997). Imaging of H_3^+ infrared emission has been used to constrain Jupiter's magnetic field parameters (Connerney et al., 1998), investigate the structure and dynamics of Jupiter's aurorae (Miller et al., 2000; Raynaud et al., 2004a), and also to probe the conditions of Jupiter's non-auroral ionosphere (Miller et al., 1997). This work details the potential to observe the effects of atmospheric gravity waves in the column emission of H_3^+ at Jupiter's mid to low latitudes.

The infrared emission of H_3^+ is a function of its vertical density profile and the temperature profile for a given location. A radiative transfer model is coupled with the wave-ionosphere model to calculate the H_3^+ column emission at each location along the horizontal phase of a propagating wave using the modeled, perturbed temperature and H_3^+ density profile. We calculate the H_3^+ emission at 3.4 μm that emerges from the top of the atmosphere and calculate an emission contrast, D, defined as the maximum to minimum variation of the observed emission, I, normalized to the emission average $I_{average}$ along the horizontal path of the wave

$$D = \frac{I_{max} - I_{min}}{I_{average}}. \quad (4)$$

The emission contrast provides a quantitative measure for the potential of the waves to be observed.

4. Model results

The perturbations of the H_3^+ density in Jupiter's ionosphere due to a propagating gravity wave give rise to horizontal variations in the H_3^+ thermal emission from the planet which results in a contrast in the observed intensity along a horizontal wavelength. Observations of the H_3^+ thermal emission from Jupiter's mid-latitudes, given sufficient spatial resolution and signal to noise, can detect this contrast. These observations can reveal typical amplitudes, wavelengths, locations, directions of propagation, source regions, as well as the frequencies of occurrence of the observable waves, leading to a more complete understanding of the waves present in Jupiter's upper atmosphere. In this section wave and planetary parameters that most strongly affect the magnitude of the variations in the H_3^+ thermal emission are investigated. The emission contrast is calculated as the percentage difference between the maximum and minimum emission along a horizontal wavelength according Eq. (4). These results help determine where on the planet will be most favorable to yield observations and waves with which parameters are most likely to be observed.

To illustrate the model results, Fig. 4 demonstrates the effect of a gravity wave on the H_3^+ structure in Jupiter's ionosphere. The wave used in this simulation is wave 1 from Young et al. (1997), extracted from the Galileo Probe temperature profile. Its amplitude is shown in the bottom left panel. The top left panel demonstrates the vertical profile of the H_3^+ density in response to the wave. This profile reveals sharp peaks and troughs in response to the forcing wave and chemical interactions with H^+ and electrons. The top right panel is the expansion of the H_3^+ density to two dimensions, illustrating the phases of the gravity wave perturbations. The boxed vertical region corresponds to the vertical profile in the adjacent left panel. The bottom right panel is the H_3^+ column emission normalized to the average emission for each point along the horizontal direction. The predicted emission contrast (maximum to minimum) for this wave is about 23%.

4.1. Wave peak altitude

The magnitude of the H_3^+ emission contrast depends, in part, on the altitude of dissipation of the wave, or the altitude at which its perturbations on the background atmosphere are greatest. This altitude depends on the parameters of the wave. Fig. 5 displays the altitude at which a wave peaks for vertical wavelengths up to 300 km and horizontal wavelengths up to 15,000 km. On the other hand the background H_3^+ density in Fig. 3 shows a well defined H_3^+ layer in the altitude region between 550 and 650 km above the 1 bar pressure level. Most of the H_3^+ thermal emission originates from this region. Gravity waves that peak in this range therefore create the largest effects on the H_3^+ density perturbation and in turn on the H_3^+ emission contrast.

The wave peak altitude is determined by the balance between the exponential growth of a wave with altitude and the increasing dissipative effects at higher altitudes. Throughout the thermosphere most of the dissipation is due to molecular viscosity and thermal conduction. The viscous dissipation is proportional to the vertical shear of the wind. The vertical shear in the winds produced by a gravity wave is directly related to the vertical wavelength. A smaller vertical wavelength yields larger vertical wind shear which results in more rapid dissipation of the wave and a lower peak altitude. Conversely, waves with larger vertical wavelengths peak at higher altitudes. The wave parameter region for which waves peak at altitudes where H_3^+ is most abundant is shown in shades of blue[1] in Fig. 5 and is bracketed between the two black curves. The two observed waves from the Galileo Probe temperature profile (Young et al., 1997) are labeled as G1 and G2 and the inferred wave from the J0 ingress electron density profile (Barrow and Matcheva, 2011) is labeled as J0 on the Figure. The parameters of these waves are described in Table 1.

Fig. 6 illustrates the dependence of the H_3^+ emission variation with respect to the vertical wavelength. For four horizontal wavelengths of 1000 km, 2000 km, 3200 km, and 10,000 km, waves with vertical wavelengths ranging from 50 km to 300 km are propagated in the model and the resulting percentage variation (peak to trough) in the H_3^+ column emission is displayed. The wavelengths between the black lines yield waves that peak at altitudes between 550 and 650 km, corresponding to the background H_3^+ density peak (the contoured region in Fig. 5). It is evident that waves with these parameters have the largest impact on the observed H_3^+ emission.

4.2. Vertical wavelength

In addition to the effect of the vertical wavelength on the wave peak altitude, the vertical wavelength itself has a direct impact on the horizontal variations in the vertically integrated H_3^+ emission. Since the effect is in the column emission, it is the integration of vertical variations that are observed. The observed horizontal contrast is diminished if the vertical wavelength is small and there are more vertical phases to average out. The observed contrast is greater if the vertical wavelength is large which minimizes the vertical averaging.

The bottom line is that waves that peak in the region of maximum H_3^+ abundance and that have a larger vertical wavelength have the best chance to be detected in the H_3^+ emission contrast. Fig. 6 also shows that waves with larger horizontal wavelengths

[1] For interpretation of color in Figs. 4–6, the reader is referred to the web version of this article.

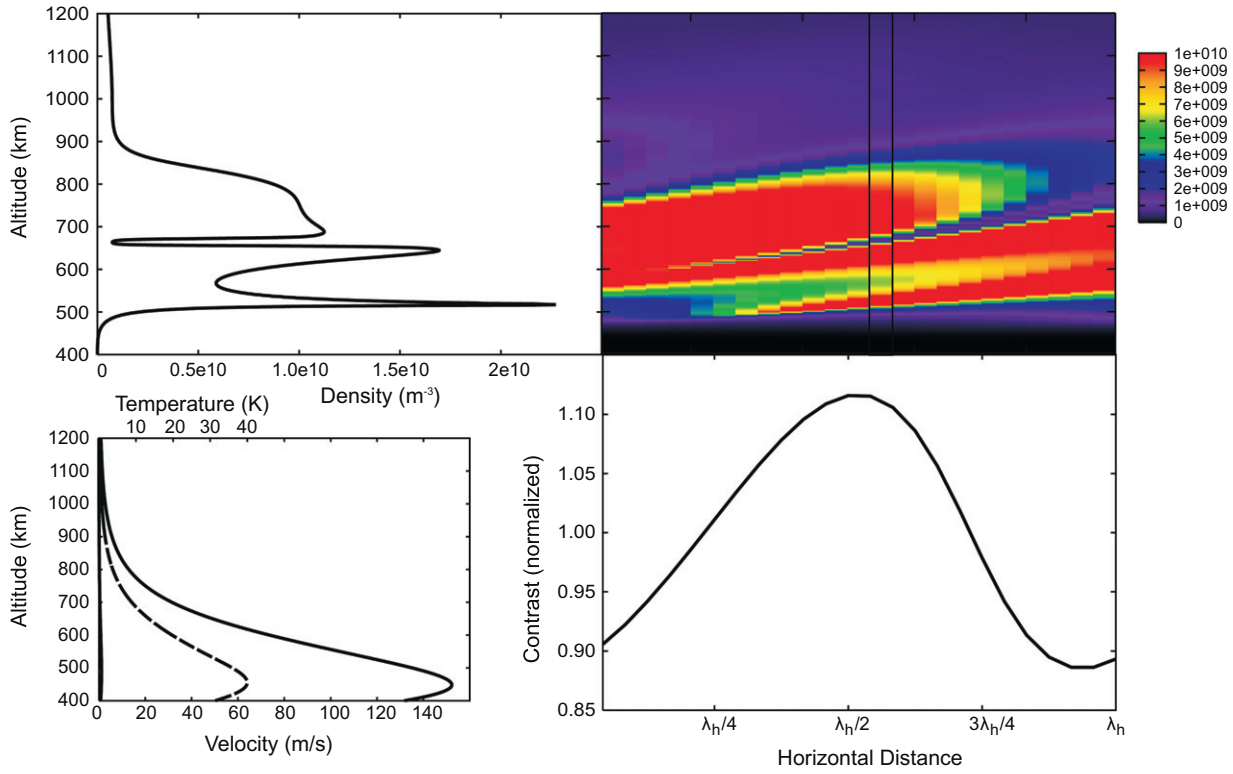

Fig. 4. Gravity wave effects on the H_3^+ density structure and emission. The Figure shows the model results for wave 1 from Young et al. (1997) interacting with Jupiter's ionosphere. The wave has horizontal wavelength of 12,693 km and a vertical wavelength of 93 km at the wave peak. The top left panel demonstrates the modeled H_3^+ density with respect to altitude after five wave periods have elapsed. The top right panel shows the full two-dimensional H_3^+ density structure in response to the wave. The velocity amplitude (solid line) and the temperature amplitude (dashed line) of the neutral wave are shown in the bottom left panel. The bottom right panel illustrates the resulting, normalized H_3^+ emission due to this wave.

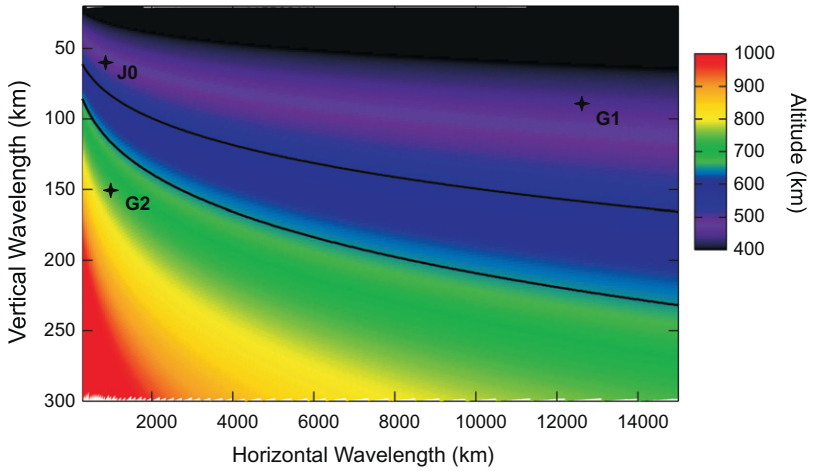

Fig. 5. Gravity wave peak altitude. The altitude at which the gravity wave amplitude is maximum for given vertical and horizontal wavelengths. The parameters of the three observed waves are indicated by the labels J0, G1, and G2 (see Table 1).

also result in a bigger emission contrast. There is a simple explanation for this: a wave with a larger horizontal wavelength requires larger vertical wavelength to propagate up to the same altitude before it dissipates (Fig. 5). Thus, for waves peaking at the same altitude (waves between the black lines in Fig. 6) larger horizontal wavelengths yield greater variations in the H_3^+ emission.

4.3. Gravity wave period

Another major factor that influences the contrast of H_3^+ emission is the period of the perturbing gravity wave. As mentioned in Section 2, when a long-lived ion species is perturbed by a gravity wave, a short-lived ion undergoes chemical interactions with the long-lived species and will establish equilibrium rather quickly. The term "short-lived" here is relative to the period of the perturbing wave. This results in significant changes in the densities of the short lived ions. The total number of short-lived ions will not be conserved in general. This can lead to large variations of the column density of the short-lived ion in the horizontal direction of the gravity wave motion. Fig. 2 illustrates the lifetime of H_3^+ and the buoyancy period, the lower limit for gravity wave periods. It is evident that while H_3^+ may have significant dynamical perturbations for

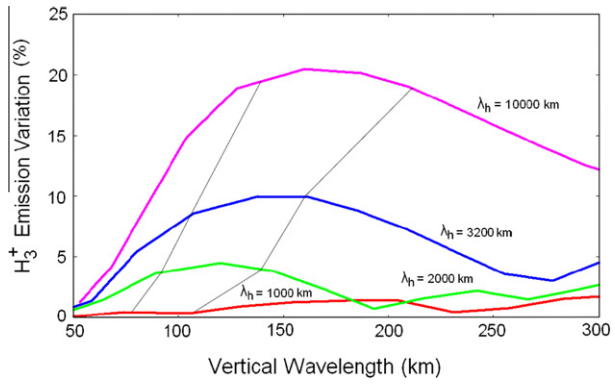

Fig. 6. Emission contrast as a function of the wave vertical and horizontal wavelength. The emission contrast is shown for four different horizontal wavelengths (λ_h = 1000 km, 2000 km, 3200 km, 10,000 km) for vertical wavelengths ranging from λ_z = 50 km to λ_z = 300 km. The waves have a 24 K amplitude at the peak. The magnetic field inclination is I = 47°. The waves between the black lines peak in the same region as the background H_3^+ density peak.

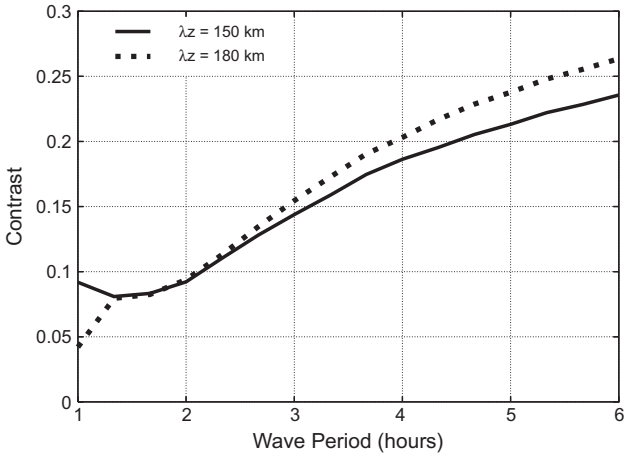

Fig. 7. Contrast dependence (Eq. (4)) on gravity wave period. The H_3^+ emission contrast is shown for waves with a span of periods ranging from 1 h to 6 h for two vertical wavelengths of 150 km and 180 km.

short period waves, for long period waves H_3^+ will be relatively short-lived, be more chemically perturbed, and have large differences in the column densities across the horizontal.

Fig. 7 illustrates the dependence of the H_3^+ emission contrast, D, with respect to wave period. To limit other effects on the emission contrast waves with temperature amplitudes of 40 K and the same vertical wavelengths are used with a range of horizontal wavelengths. The horizontal wavelengths used range from about 1000 km to 5000 km and result in waves with periods from about 1 h to 6 h. Fig. 7 demonstrates that H_3^+ emission contrast increases as the wave period increases, an expected result as H_3^+ effectively becomes a short-lived ion. For short period waves H_3^+ is primarily dynamically perturbed at altitudes near the H_3^+ density peak. In this situation the H_3^+ ions are largely conserved and there is relatively little horizontal variation in the H_3^+ column density. In contrast, for long period waves the H_3^+ lifetime is small compared to the wave period and these ions tend toward chemical equilibrium with the long-lived H^+ ions and electrons. In this situation there is no conservation imposed on the H_3^+ ions and the H_3^+ column density can vary significantly across the horizontal plane.

4.4. Ion perturbation amplitude

The previous sections described how the emission contrast is affected by the spectral characteristics of a gravity wave. Another factor that strongly affects the emission contrast is the degree to which the ions are perturbed by the wave. The amplitudes of the ion perturbations are strongly dependent on several independent factors, including the amplitude of the forcing wave, the direction of wave propagation, and the inclination of the magnetic field lines.

The observable effect in the H_3^+ emission is very sensitive to the amplitude of the gravity wave. A gravity wave with a larger amplitude has greater velocity perturbations which yield stronger forcing of the ions and larger ion density perturbations.

4.4.1. Wave propagation direction

The direction of wave propagation relative to the magnetic field orientation strongly affects the magnitude of the ion perturbation. In the gravity wave-ionosphere perturbation mechanism (Section 2) the ion velocity is constrained to the magnetic field lines and is thus a projection of the neutral winds onto the magnetic field lines. For simplicity Fig. 1 assumes that the neutral velocity $\vec{U}_n$ and the local magnetic field both have the same horizontal orientation. The ion velocity projections are maximum when the neutral

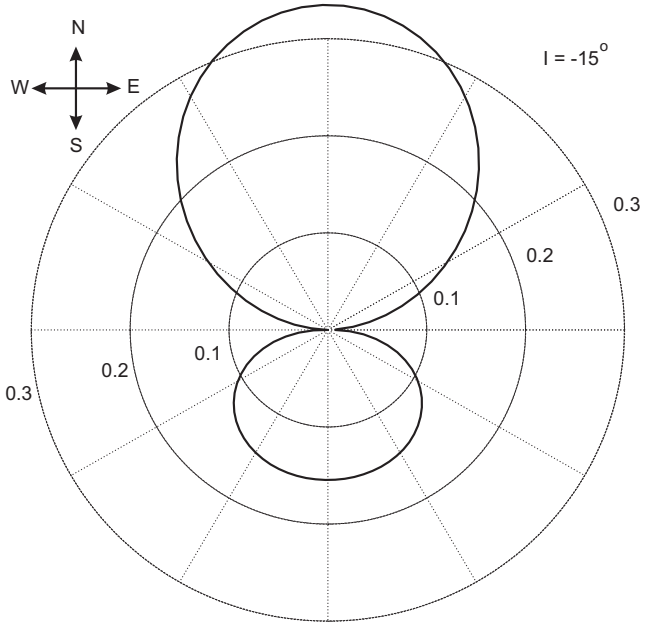

Fig. 8. Ion perturbation dependence on the direction of wave propagation. The wave phase plane is inclined at 8° with respect to the horizontal plane. The magnetic field inclination is −15°, which corresponds to −15° magnetic latitude.

velocity and the magnetic field have the same horizontal orientation and are minimum when the horizontal orientations are perpendicular. In the minimum case the ion velocities are due solely to the projections of the vertical component of the neutral velocity onto the magnetic field lines. In the hydrostatic limit, the vertical wind component of a gravity wave is small compared to the horizontal wind component, which results in relatively small ion density perturbations for waves with horizontal phase velocity perpendicular to the horizontal magnetic field orientation.

Fig. 8 shows the relative magnitude of the ion density perturbation for a wave propagating in different horizontal directions (Eq. (2)). The wave shown is a small amplitude wave with λ_h = 1000 km and λ_z = 130 km at the wave peak altitude. The inclination is negative, which corresponds to Jupiter's northern hemisphere. It is apparent that the largest ion perturbations occur for waves propagating along the magnetic meridian. For small inclinations, at mid-low latitudes, the ion perturbations are greatest for waves

propagating away from the equator. Waves propagating off-meridian will have their resulting ion density perturbation amplitudes reduced as shown in Fig. 8.

4.4.2. Latitude (magnetic field inclination)

The magnetic field orientation, and thus the location on the planet, strongly affects the magnitude of the wave-induced ionospheric perturbations. It is seen in the geometry of Fig. 1 that when the phase lines of the wave are parallel to the magnetic field there is no separation of the neutral and ion velocities and since hydrostatic gravity waves are non-compressible the ion motion is non-divergent too. Alternatively when the neutral winds are perpendicular to the magnetic field the ions cannot follow the motion of the neutrals as they are constrained to the magnetic field lines. In both cases ion density perturbations due to a gravity wave are absent.

In addition, the ionospheric response to gravity waves depends on the structure of the background ionosphere in general and any factor that impacts the steady state ion distribution will also modify the magnitude of the wave-induced effects. As the magnetic field inclination changes with latitude so does the ion diffusion velocity which impacts mostly the top of the ionosphere. The photoproduction of ions is also latitudinally dependent as the zenith angle of the incident solar flux changes with latitude. The resulting latitudinal dependence of the location and the thickness of the H_3^+ layer affects the magnitude of the H_3^+ density perturbations and thus translates into a latitudinal dependence of the emission contrast as well.

4.5. Expected emission contrast for observed waves

Though few in number, there are several observations of gravity waves at Jupiter's ionospheric heights. In this section these waves are used to calculate what contrast one would expect to observe for these known wave parameters. Three observed waves are used: two from the temperature profile retrieved by the Galileo Probe (Young et al., 1997) and the modeled wave used to fit the sharp layers in the J0-ingress electron density profile (Barrow and Matcheva, 2011). The parameters of these waves are listed in Table 1 along with the model calculated emission contrast. For the Galileo Probe waves, amplitudes of 40 K are used corresponding to the calculated amplitudes in Young et al. (1997). The J0-ingress wave has a relatively small vertical wavelength and therefore cannot sustain these large amplitudes without breaking; the amplitude used for this wave is 25 K.

The results can be interpreted in light of the results in the previous sections. The Galileo Probe wave 1 (G1) reveals a very large emission contrast of 23%, well within the expected observable regime. This large contrast is due to two main factors: the long wave period Section 4.3) and that the wave peaks below the main H_3^+ density peak but still has a significant amplitude at the H_3^+ density maximum. Because the ion densities drop off sharply below the density peak, the ion perturbations occur in a smaller vertical band (at the density peak) which results in less vertical averaging in the column emission calculation. The Galileo Probe wave 2 (G2) demonstrates a modest emission contrast of only 5%. This smaller contrast is due to the very short wave period and to the fact that the wave has a maximum 200 km above the main H_3^+ density peak. The J0-ingress wave shows a very small contrast of less than 1%. This wave has a short period and a small vertical wavelength so it is not well suited to be observed via this method.

Three sample waves were also analyzed to determine the potential for observability of waves with similar parameters. These waves were chosen by making small alterations to the observed wave parameters intending to enhance the observability and are denoted by asterisks in Table 1. For Galileo Probe wave 1 the vertical wavelength was increased by roughly 50%, increasing the wave peak altitude by 50 km. Although the expected contrast for this wave was already large, a larger vertical wavelength for this wave creates a somewhat larger contrast of 28.7%. The Galileo Probe 2 wave was changed to have a longer wave period, increased by roughly a factor of two, which also results in a larger horizontal wavelength and a wave peak altitude 100 km lower. The effect of this change enhanced the emission contrast more than threefold. The altered J0-ingress wave has the same peak altitude but the wavelengths and period have each been increased dramatically in order to generate a wave with significant contrast.

Although there are few observed waves at Jupiter's ionospheric heights, the results demonstrate that at least two of these waves could have generated an observable contrast in the H_3^+ thermal emission. Further, the parameters of the observed waves span a large range of periods, wavelengths, and peak altitudes. This leads to the expectation that waves with a variety of parameters exist, many of which have been shown to generate emission contrast in the observable range.

5. Concluding remarks

The current work demonstrates the observability of atmospheric gravity waves in Jupiter's upper atmosphere by monitoring the planet's near infrared emission at 3.4 μm. We use an atmospheric gravity wave model coupled with ionospheric chemistry and dynamics to calculate the vertical and horizontal distribution of H_3^+ ions for a given set of wave parameters. The output is used to estimate the vertically integrated thermal emission coming from H_3^+ ions. We explore a large range of wave parameters and investigate which factors impact the observed effect.

In terms of the predominant mechanism that creates perturbations in the local H_3^+ density we distinguish two wave regimes: waves with periods comparable to the lifetime of H_3^+ ions and waves with periods that are long with respect to the H_3^+ lifetime. In the case of waves with short periods the H_3^+ ions are moved mechanically along the magnetic field lines, the ion column density is conserved along the wave path and little to no variation is expected in the observed H_3^+ emission along the wave path. For long-period waves fast chemical reactions (electron recombination and charge exchange reactions) maintain the H_3^+ chemical equilibrium along the path of wave propagation and as a result the ion column density is not conserved. This leads to observable signatures in the vertically integrated H_3^+ emission.

The impact on the observed H_3^+ emission is optimized for waves with large vertical and horizontal wavelengths that achieve maximum amplitude at or near the hight of maximum H_3^+ density (roughly 550 km above the 1 bar pressure level). Larger effect is expected from waves with larger amplitudes. Waves that travel in the north/south direction are easier to detect than waves propagating zonally. The model also predicts that the largest signal is to come from waves present at middle latitudes.

Waves with parameters consistent with the Galileo Probe temperature profile (Young et al., 1997) can leave observable signatures in the H_3^+ thermal emission resulting in 5–23% emission contrast along the horizontal path of the wave.

To apply the technique described in this paper for detecting atmospheric gravity waves, several constraints need to be combined: highly sensitive spectral images or narrow spectral band images have to be repeated in L band at a repetition rate high enough to sample the period of the gravity wave. The spatial extension of the wave, although not fully known, needs a spatial resolution at a regional scale for the wave to be horizontally resolved. In that sense a space observatory would be more adequate since a better space resolution can be achieved. One of the science

objectives of the JUNO/JIRAM instrument (Adriani et al., 2008) is to search for gravity waves from H_3^+ modulation in the non-auroral regions of Jupiter. High frequency waves (short periods) tend to propagate higher in the atmosphere as they are less impacted by dissipation however they result in smaller impact on the H_3^+ emission and the amplitude of the predicted contrast is small.

The gravity waves considered in this work are linear with the wave amplitude being always less than the critical value so that no wave breaking occurs. In reality if a wave propagates up to high altitudes (assuming that the wave does not encounter critical levels or gets reflected, and does not get strongly dissipated due to viscosity) there is nothing to preclude the wave amplitude to grow until the wave breaks and overturns. Numerical simulations and terrestrial observations suggest that overturning of the wave occurs in narrow bands along the phase lines where the local temperature gradient exceeds the adiabatic lapse rate. In these bands the mixing of the air is increased limiting the accumulation of ions along the magnetic field line. A detailed modeling of the gas dynamics is needed to understand and quantify the ion motion in a wave breaking region.

Acknowledgments

This work is supported by NASA under Grant NNX07AF29G issued through the Planetary Atmospheres program. The authors thank Kunio Sayanagi and an anonymous reviewer for their constructive suggestion to improve the manuscript.

References

Adriani, A. et al., 2008. JIRAM, the image spectrometer in the near infrared on Board the Juno Mission to Jupiter. Astrobiology 8, 613–622.
Arregi, J., Rojas, J.F., Hueso, R., Sanchez-Lavega, A., 2009. Gravity waves in Jupiter's equatorial clouds observed by the Galileo orbiter. Icarus 202, 358–360.
Atreya, S.K., Donahue, T.M., Sandel, B.R., Broadfoot, A.L., Smith, G.R., 1979. Jovian upper atmospheric temperature measurement by the Voyager 1 UV spectrometer. Geophys. Res. Lett. 6, 795–798.
Ballester, G.E., Miller, S., Tennyson, J., Trafton, L.M., Geballe, T.R., 1994. Latitudinal temperature variations of jovian H_3^+. Icarus 107, 189–194.
Barrow, D., Matcheva, K.I., 2011. Impact of atmospheric gravity waves on the jovian ionosphere. Icarus 211, 609–622.
Connerney, J.E.P., Acuña, M.H., Ness, N.F., Satoh, T., 1998. New models of Jupiter's magnetic field constrained by the Io flux tube footprint. J. Geophys. Res. 103, 11929–11940.
Cravens, T.E., 1987. Vibrationally excited molecular hydrogen in the upper atmosphere of Jupiter. J. Geophys. Res. 92, 11083–11100.
Davis, M.J., 1973. The integrated ionospheric response to inertial atmospheric gravity waves. J. Atmos. Terr. Phys. 35, 929–959.
Drossart, P. et al., 1989. Detection of H_3^+ on Jupiter. Nature 340, 539–541.
Drossart, P., Maillard, J.-P., Caldwell, J., Rosenqvist, J., 1993. Line-resolved spectroscopy of the jovian H_3^+ auroral emission at 3.5 micrometers. Astrophys. J. Lett. 402, L25–L28.
Fjeldbo, G., Kliore, A., Seidel, B., Sweetnam, D., Cain, D., 1975. The Pioneer 10 radio occultation measurements of the ionosphere of Jupiter. Astron. Astrophys. 39, 91–96.
French, R., Gierasch, P.J., 1974. Waves in the jovian upper atmosphere. J. Atmos. Sci. 31, 1707–1712.
Friedson, A.J., 1999. New observations and modelling of a QBO-like oscillation in Jupiter's stratosphere. Icarus 137, 34–55.
Harrington, J., French, R.G., Matcheva, K.I., 2010. The 1998 November 14 occultation of GSC 0622-00345 by Saturn – II: Stratospheric Thermal profile, power spectrum, and gravity waves. Astrophys. J. 716, 404–416.
Hickey, M.P., Walterscheid, R.L., Schubert, G., 2000. Gravity wave heating and cooling in Jupiter's thermosphere. Icarus 148, 266–281.
Hinson, D.P., Flasar, M.F., Kliore, A.J., Schinder, P.J., Twicken, J.D., Harrera, R.G., 1997. Results from the first Galileo radio occultation experiment. J. Geophys. Res. Lett. 24, 2107–2110.
Hooke, W.H., 1968. Ionospheric irregularities produced by internal atmospheric gravity waves. J. Atmos. Terr. Phys. 30, 795–823.
Hooke, W.H., 1970. The ionospheric response to internal gravity waves – 1: The F2 region response. J. Geophys. Res. 75, 5535–5544.
Hunt, G.E., Muller, J.-P., 1979. Voyager observations of small-scale waves in the equatorial region of the jovian atmosphere. Nature 280, 778–780.
Hunten, D.M., Dessler, A.J., 1977. Soft electrons as a possible heat source for Jupiter's thermosphere. Planet. Space Sci. 25, 817–821.
Kao, L., Oka, T., Miller, S., Tennyson, J., 1991. A table of astronomically important rovibrational transitions for the H_3^+ molecular ion. Astrophys. J. Suppl. Ser. 77, 317–329.
Kirchengast, G., 1996. Elucidation of the physics of the gravity wave–TID relationship with the aid of theoretical simulations. J. Geophys. Res. 101, 13353–13368.
Leovy, C.B., Friedson, A.J., Orton, G.S., 1991. The quasiquadrennial oscillation of Jupiter's equatorial stratosphere. Nature 354, 380–382.
Matcheva, K.I., Strobel, D.F., 1999. Heating of Jupiter's thermosphere by dissipation of gravity waves due to molecular viscosity and heat conduction. Icarus 140, 328–340.
Matcheva, K.I., Strobel, D.F., Flasar, F.M., 2001. Interaction of gravity waves with ionospheric plasma: Implications for Jupiter's ionosphere. Icarus 152, 347–365.
Melin, H., Miller, S., Stallard, T., 2005. Non-LTE effects on H_3^+ emission in the jovian upper atmosphere. Icarus 178, 97–103.
Miller, S., 2000. Infrared spectroscopic studies of the jovian ionsophere and aurorae. Adv. Space Res. 26, 1477–1488.
Miller, S., Achilleos, N., Ballester, G.E., Lam, H.A., Tennyson, J., Geballe, T.R., Trafton, L.M., 1997. Mid-to-low latitude H_3^+ emission from Jupiter. Icarus 130, 57–67.
Niemann, H.B. et al., 1996. The Galileo Probe mass spectrometer: Composition of Jupiter's atmosphere. Science 272, 846–849.
Nishida, A., Watanabe, Y., 1981. Joule heating of the jovian ionosphere by corotation enforcement currents. J. Geophys. Res. 86, 9945–9952.
Raynaud, E., Drossart, P., Matcheva, K., Sicardy, B., Hubbard, W.B., Roques, F., Widemann, T.H., Gladstone, G.R., Waite, J.H., Nadeau, D., Bastien, P., Doyon, R., Hill, R., Rieke, M.J., Marley, M., 2003. The 10 October 1999 HIP 9369 occultation by the northern polar region of Jupiter: Ingress and egress lightcurves analysis. Icarus 162, 344–361.
Raynaud, E., Lellouch, E., Maillard, J.-P., Gladstone, G.R., Waite, J.H., Bezard, B., Drossart, P., Fouchet, T., 2004a. Spectro-imaging observations of Jupiter's 2-μm auroral emission – I: H_3^+ distribution and temperature. Icarus 171, 133–152.
Raynaud, E., Matcheva, K., Drossart, P., Roques, F., Sicardy, B., 2004b. A re-analysis of the 1971 Beta Scorpii occultation by Jupiter: Study of temperature fluctuations and detection of wave activity. Icarus 168, 324–335.
Reuter, D.C. et al., 2007. Jupiter cloud composition, stratification, convection, and wave motion: A view from New Horizons. Science 318, 223–225.
Sayanagi, K.M., Showman, A.P., 2007. Effects of a large convective storm on Saturn's equatorial jet. Icarus 187, 520–539.
Schubert, G., Hickey, M.P., Walterscheid, R.L., 2003. Heating of Jupiter's thermosphere by the dissipation of upward propagating acoustic waves. Icarus 163, 398–413.
Seiff, A. et al., 1997. Thermal structure of Jupiter's upper atmosphere derived from the Galileo Probe. Science 276, 102–104.
Seiff, A. et al., 1998. Thermal structure of Jupiter's atmosphere near the edge of a 5-μm hot spot in the north equatorial belt. J. Geophys. Res. E103, 22857–22890.
Shemansky, D.E., 1985. An explanation for the H Ly-alpha longitudinal asymmetry in the equatorial spectrum of Jupiter – An outcrop of paradoxical energy deposition in the exosphere. J. Geophys. Res. 90, 2673–2694.
Simon-Miller, A.A., Conrath, B.J., Gierasch, P.J., Orton, G.S., Achterberg, R.K., Flasar, F.M., Fisher, B.M., 2006. Jupiter's atmospheric temperatures: From Voyager IRIS to Cassini CIRS. Icarus 180, 98–112.
Simon-Miller, A.A., Poston, B.W., Orton, G.S., Fisher, B., 2007. Wind variations in Jupiter's equatorial atmosphere: A QQO counterpart? Icarus 186, 192–203.
Stallard, T., Miller, S., Millward, G., Joseph, R.D., 2002. On the dynamics of the jovian ionosphere and thermosphere – II: The measurement of H_3^+ vibrational temperature, column density, and total emission. Icarus 156, 498–514.
Strobel, D.F., 1979. The Galilean satellites as a source of CO in the jovian upper atmosphere. Icarus 37, 256–263.
Strobel, D.F., Smith, G.R., 1973. On the temperature of the jovian thermosphere. J. Atmos. Sci. 30, 718–725.
von Zahn, U., Hunten, D.M., Lehmacher, G., 1998. Helium in Jupiter's atmosphere: Results from the Galileo Probe helium interferometer experiment. J. Geophys. Res. 103, 22815–22830.
Waite, J.H. et al., 1997. Equatorial X-ray emissions: Implications for Jupiter's high exospheric temperatures. Science 276, 104–108.
Waite, J.H., Cravens, T.E., Kozyra, J., Nagy, A.F., Atreya, S.K., Chen, R.H., 1983. Electron precipitation and related aeronomy of the jovian thermosphere and ionosphere. J. Geophys. Res. 88, 6143–6163.
Yelle, R.V., Young, L.A., Vervack, R.J., Young, R., Pfister, L., Sandel, B.R., 1996. Structure of Jupiter's upper atmosphere: Predictions for Galileo. J. Geophys. Res. 101, 2149–2162.
Young, L.A., Yelle, R.V., Young, R., Seiff, A., Kirk, D.B., 1997. Gravity waves in Jupiter's thermosphere. Science 267, 108–110.
Young, L.A., Yelle, R.V., Young, R., Seiff, A., Kirk, D.B., 2005. Gravity waves in Jupiter's stratosphere, as measured by the Galileo ASI experiment. Icarus 173, 185–199.